Influence of reaction conditions and kinetic analysis of the selective hydrogenation of oleic acid toward fatty alcohols on Ru-Sn-B/Al$_2$O$_3$ in the flow reactor

V.O. Rodina [a,*], D. Yu. Ermakov [a], A.A. Saraev [a,b], S.I. Reshetnikov [a], V.A. Yakovlev [a,b,c]

[a] Boreskov Institute of Catalysis SB RAS, Lavrentieva Ave. 5, 630090 Novosibirsk, Russia
[b] Novosibirsk State University, Pirogova Str. 2, 630090 Novosibirsk, Russia
[c] UNICAT Ltd., Lavrentieva Ave. 5, 630090 Novosibirsk, Russia

A R T I C L E   I N F O

A B S T R A C T

The hydrogenation of oleic acid (*cis*-9-octadecenoic acid) into oleyl alcohol (methyl-9-octadecen-1-ol) was studied in the presence of a bimetallic RuSn supported over alumina catalyst in the flow reactor. It was shown that the process should be performed at the temperature range of 280–330 °C, hydrogen pressure of 3.5–5.3 MPa and contact time less than 0.2 h in order to obtain the highest possible yield of desired products (fatty alcohols and waxes). The study by physicochemical methods (XRD, BET, TPR, XPS, TEM) revealed that modification of the catalyst with boron promotes additional simultaneous reduction of the major part of tin and ruthenium oxides, most of which are reduced below 310 °C. Crystalline Ru$_x$Sn$_y$ structures with variable composition, which seem to be the active component of the selective hydrogenation catalyst, were found to be formed after the reaction at temperatures higher than 300 °C. Our work demonstarted that a scheme of oleic acid transformations includes formation of waxes by recombination of carboxyl and alkanes intermediates, acid decarboxylation and hydrocracking of waxes to alkanes. Mathematic simulation methods allowed us to estimate rate constants of the process stages and the main kinetic parameters (Ea, k$_0$).

1. Introduction

Nowadays lipids obtained from vegetable sources are used both for the production of biofuels and for the synthesis of oxygenated chemicals, such as fatty alcohols, aldehydes and ketones. Fatty alcohols are the most valuable products in this list. Together with their derivatives they are essential ingredients in the production of consumer chemicals and cosmetics. They are present in the recipes of detergents, shampoos and creams. In 2007 the world consumption of fatty alcohols was 1.92 million tons with the annual production volume of 2 million tons [1]. By 2012 the world production of fatty alcohols reached 3.35 million tons [2]. Today more than a half of produced fatty alcohols are made from vegetable sources.

The development of catalytic hydrogenation makes production of natural fatty alcohols from renewable sources, such as fats, oils (*e.g.* coconut, palm, rape, soybean) and their derivatives, more important. Generally, in industry this process is carried out over zinc chromite catalysts, but the low activity of these materials requires severe conditions of temperature (250–300 °C) and pressure (20–35 MPa) [3,4]. The process is based on the hydrogenation of fatty acids and their methyl esters, which are produced by transesterification of vegetable oils or animal fats. Several attempts have been made to develop suitable catalytic systems operating at less severe conditions. More recently, the catalysts containing a noble metal (Rh, Ru, Pd, Ru) were described for the selective reduction of fatty esters to alcohols, especially, unsaturated ones [5–9]. High yield of fatty alcohols exceeding 95% of the theoretical value is the main advantage of this process [10–15]. Its main drawbacks are the use of multistage and high pressure.

The activity and selectivity of these catalysts is enhanced by selection of the appropriate supports and promoters [10,13]. There are some reviews reporting that the addition of tin to different noble metals could give a strong improvement of the selectivity toward alcohols depending on the way of tin modifiers introduction [12,16–18]. It was shown [13] that methyl oleate could be selectively hydrogenated into oleyl alcohol in the presence of a mixed ruthenium–tin–boron catalyst based on alumina support (4.5 MPa, 270 °C). It was reported a selectivity of about 80% at a conver-

* Corresponding author.
E-mail address: dundich@catalysis.ru (V.O. Rodina).

sion of 80% when a RuSnB/Al$_2$O$_3$ (with Sn/Ru = 2) was prepared by impregnation of alumina with chlorides followed by the reduction with sodium borohydride. Mizukami and co-workers [11,12] also claimed that Ru–Sn system is a selective catalyst for the formation of oleyl alcohol. Pouilloux and co-workers [14–16] demonstrated that the process of the methyl oleate hydrogenation could be more complex than it is generally proposed. It was shown that a trans-esterification of methyl oleate (the reagent) and oleyl alcohol (one of the primary products) occurs with the formation of heavy esters [19]. Such esters are also adsorbed on the catalyst surface and transformed to oleyl alcohol. This result was taking as a basis for the present study.

In the literature, the synthesis of fatty alcohols based on vegetable lipids treatment has been mostly studied in batch reactors: different catalytic systems have been used, and process conditions have been determined [13–17]. Meanwhile, for industrial implementation it is preferable to organize the process in the flow mode. Therefore, it is necessary to study the selective hydrogenation of fatty acid derivatives made from vegetable sources under flow conditions. To obtain high yields of the desired products, it is important to determine optimum process conditions and main kinetic parameters, which was the main goal of this study.

2. Experimental

2.1. Materials

Oleic acid («Reachem», 99+%), sodium borohydride (99+%), Ruthenium (III) chloride (99+%) and SnCl$_2$·6H$_2$O («Reachem», 99+%) were used as received. Spherical particles Al$_2$O$_3$ with a diameter of 0.2–0.8 mm were obtained from «SKTB Catalyst» (T$_{tempering}$ = 1000 °C, area 159 m^2/g).

2.2. Catalysts preparation

All the solids were prepared by coimpregnation of the support (Al$_2$O$_3$) with aqueous solution containing RuCl$_3$ and SnCl$_2$, according to the method described by Narasimhan et al. [13]. The catalysts were prepared as follows: 0.16 g of RuCl$_3$·xH$_2$O and 0.30 g of SnCl$_2$·2H$_2$O were separately dissolved in 7.5 ml of water and then mixed in a beaker. 5 g of γ-alumina was impregnated with the above solution by the conventional incipient wetness technique. Before the catalyst preparations, Al$_2$O$_3$ was calcined in air at 1000 °C. After the impregnation step (16 h), the impregnated samples were reduced with an aqueous solution of sodium borohydride (1.1 g). Then the solids were filtered, washed with water and ethanol and dried at 80 °C under nitrogen for 4 h. The resulting RuSnB/Al$_2$O$_3$ were placed in an oven at 80 °C and dried under a flow of nitrogen at 120 °C for 4 h. Before use, all catalysts prepared by coimpregnation were reduced with hydrogen at 300 °C.

2.3. Catalysts characterization

2.3.1. Transmission electron microscopy (TEM)

Transmission electron microscopy (TEM) measurements were performed on a JEM 2010 microscope (JEOL, Japan) at an accelerating voltage of 200 kV with 0.14 nm resolution. Before being examined, the sample was reduced in a hydrogen atmosphere and was passivated with ethanol. The microanalysis of Ru and Sn was carried out by energy dispersive X-ray spectroscopy (EDX) in the nanoprobe mode.

2.3.2. Temperature-programmed reduction (TPR)

Temperature-programmed reduction (TPR) experiments were performed in a conventional flow setup, the gas phase analysis

being made with a thermal conductivity detector (TCD). The Ru-Sn-B/Al$_2$O$_3$ catalyst (0.01 g) was placed in a U-tube quartz reactor and heated in a reducing atmosphere (10 vol% of H$_2$ balanced in argon at a flow rate of 20 ml/min) up to 800 °C with a constant heating rate of 4 °C/min.

The specific surface area of samples were determined with the Brunauer–Emmett–Teller (BET) method using nitrogen adsorption isotherms measured at liquid nitrogen temperatures with an automatic volumetric adsorption unit ASAP 2400 (Micromeritics Instrument. Corp., USA). Before each measurement, the samples were degassed for 4 h under vacuum at 150 °C.

2.3.3. X-ray diffraction (XRD)

X-ray diffraction (XRD) of the fresh catalysts was studied *ex situ* with a diffractometer D500 Siemence (Germany) using monochromatic CuK$_\alpha$ radiation (λ = 154.18 p.m.). The diffraction patterns were recorded in steps of 0.05° with a count time of 3 s in the 2θ range of 30–80°.

The chemical analysis of the catalyst surface was performed using X-ray photoelectron spectroscopy (XPS). The XPS measurements were performed on a SPECS's Surface Nano Analysis GmbH (Germany) photoelectron spectrometer equipped with a PHOIBOS-150-MCD-9 hemispherical electron energy analyzer, a FOCUS-500X-ray monochromator, and an XR-50M X-ray source with a double Al/Ag anode. The spectrometer was also equipped with a high-pressure cell (HPC) which enables to heat samples before analyzing in gaseous mixtures at pressures up to 0.5 MPa. The XPS spectra were obtained using the monochromatic AlK$_\alpha$ radiation (hn = 1486.74 eV). Binding energies of the photoemission peaks were corrected to the Al2p peak at 74.40 eV corresponding to aluminum. Relative element concentrations were determined from the integral intensities of XPS peaks using the cross-sections according to Scofield [20]. For detailed analysis the spectra were fitted into several peaks after the background subtraction by the Shirley method. The fitted procedure was performed using the CasaXPS software. The line shapes were approximated by the deconvolution of Gaussian and Lorentz functions. Before the XPS analysis, the catalysts were additionally reduced in 1 bar H$_2$ at 280, 310 and 360 °C in the HPC.

2.4. Catalysts performance

The selective hydrogenation was studied in the gas phase in a tubular fixed-bed flow reactor. The reactor was made of stainless steel (inner diameter 14 mm, length 300 mm). It was heated with an electrical furnace and the temperature was monitored with a thermocouple in the reactor. The experiments were carried out at P = 2–8 MPa and T = 250–400 °C. The feed rates of hydrogen and argon were 20 and 3 l/h, respectively. Oleic acid was used as the substrate. The substrate feed rate, U, was 3 ml/h, the contact time, τ, was varied from 0.1 to 1.67 h, and the catalyst volume, V$_{cat}$, was 5 cm^3. Before the experiments the catalysts (fraction 0.8/1.0 mm) were reduced in the reactor at 300 °C in a hydrogen flow at 8 MPa for 1 h. Then the reactor was cooled to the desired temperature, and the substrate was added to the feed. The liquid phase was sampled at least once an hour.

2.5. Analysis of reaction products

The product composition was analyzed in the liquid phase using a GC–MS spectrometer Saturn 2000 equipped with a quartz capillary column HP-5 ms (stationary phase: 5% phenyl + 95% dimethylpolysiloxane, length 30 m, inner diameter 0.25 mm). Quantitative analysis of the liquid products was carried out using an Agilent Technologies 7820A chromatograph equipped with a Zebron ZB-5 HT Inferno capillary column (stationary phase: 5%

phenyl + 95% dimethylpolysiloxane, length 30 m, internal diameter 0.32 mm, phase thickness 0.25 μm).

Also the composition of the liquid products was carried out by NMR ^{1}H analysis (Bruker Advance 400, 400.13 MHz). Liquid samples were dissolved in deuterated chloroform (CDCl$_3$) before the NMR study. The spectra were accumulated from 64 scans at the relaxation delay of 1 s.

Analysis of the reaction products by GC and NMR identified the number of compounds, such as fatty alcohols (RCH$_2$OH), heavy esters (RCOOR), normal alkanes, fatty acids, ketones (RC(O)R), and aldehydes (RC(O)H). The complete analysis of liquid compounds using GC only was complicated because of high fatty alcohols and waxes boiling temperatures ($\geq$350 °C). Despite the use of the NMR analysis only did not result in identification of the length of hydrocarbon chain or the length of oxygen-containing compounds, its combination with GC allowed us to determine quantitatively the content of the 4 groups of products differed by functional groups (fatty alcohols, heavy esters, normal alkanes, and free fatty acids) without any separation of individual compounds.

2.6. Measurement of catalyst performance

The catalyst efficiency was evaluated according to the conversion X_R (mol%) of the initial substrate, which was calculated as follows:

$$X_R = \frac{\sum n_i - n_R}{\sum n_i} \cdot 100\%$$

Selectivity S_i toward a products group i was determined as a percent of this products (alcohol, alkane, wax) in the liquid phase:

$$S_i = \frac{n_i}{(\sum n_i) - n_R} \cdot 100\%$$

The yield of the products group (i) is then defined as: $Y_i = S_i * X_R / 100\% = \frac{n_i}{\sum n_i} \cdot 100\%$ Here, n_i is mole concentration of products of group "i", $\sum n_i$ is the sum of moles of all substances at the reactor outlet including all reaction products and unreacted acid, n_R is the amount of unreacted acids (mole).

3. Results and discussion

3.1. Catalysts characterization

The elemental analysis of as prepared (non-reduced) Ru-Sn-B/Al$_2$O$_3$ showed that the catalyst contained 0.8 wt% of ruthenium, 1.8 wt% of tin, and 0.3 wt% of boron. According to N$_2$ physisorption analysis the specific surface area (A$_{BET}$) of this catalyst is equal to 149 m^2/g, while it's pore volume (V$_{pore}$) is 0.39 cm^3/g.

As prepared catalyst and the sample after reduction by hydrogen were studied by XRD, but there were not any clear reflections in the XRD pattern. However, the presence of broadened peaks can indicate small size of the catalyst particles.

3.1.1. Transmission electron microscopy (TEM)

Ru-Sn-B/Al$_2$O$_3$ catalyst was studied by transmission electron microscopy (TEM) before and after reduction as well as after reaction. Before reduction the catalyst contained Ru and Sn deposited on the γ-Al$_2$O$_3$ surface in the atomic state. Large truly amorphous non-crystalline Ru$_x$Sn$_y$ aggregates larger that 100 nm were formed on the catalyst surface after reduction at the temperature of 300 °C. In addition, Ru$_x$Sn$_y$ clusters with the size under 1 nm were observed in a great number on the surfaces of the γ-Al$_2$O$_3$ support and amorphous particles. During the reaction the truly amorphous non-crystalline particles were transformed into large crystalline ruthenium-tin aggregates, which size depended on the reaction temperature. Aggregates with dimensions 100–150 nm were observed on the catalyst surface at the reaction temperatures below 350 °C (Fig. 1a). When the reaction temperature was increased to 400 °C, larger aggregates with the size of 100–500 nm were formed by agglomeration (Fig. 1b). As it was noted above, the agglomeration process is one of the main causes of deactivation of metal catalysts [21]. Based on the obtained results, one can predict that the activity of the Ru-Sn-B/Al$_2$O$_3$ catalyst will be higher at the reaction temperatures not exceeding 350 °C.

It is difficult to determine the composition of the crystalline Ru$_x$Sn$_y$ aggregates based on the TEM data. Nevertheless, some crystalline forms of the active component were identified by studying selected areas on the surface and comparing the interplanar spacings with integral energy dispersion spectra. According to the EDX data the atomic ratio of Ru and Sn is equal to approximately 27/71 for the particle shown in Fig. 2 with the observed interplanar spacings of 3.00, 2.51 and 1.86 Å. Based on the XRD database this particle can be identified as Ru$_3$Sn$_7$ crystalline structure (2.9580 Å (310), 2.5010 Å (321), 1.9090 Å (422)). Certain discrepancy between the interplanar spacings observed for the Ru$_3$Sn$_7$ particle and reported in the database can be related to the presence of boron in the structure of the bimetallic particle. It is worth mentioning that the formation of Ru-Sn alloys [14,22,23] and Ru$_3$Sn$_7$ crystalline phase [24] being the active component of the catalysts and accounting for selective reduction of fatty acid derivatives has been already reported in the literature before.

Overall, the TEM data indicate that the morphology of the active component of Ru-Sn-B/Al$_2$O$_3$ catalyst changes with the reaction temperature increase: Ru$_x$Sn$_y$ amorphous aggregates transform to crystalline structures, which are then undergo sintering. Note that such processes can directly influence the catalyst activity and change the contributions of the different reaction pathways.
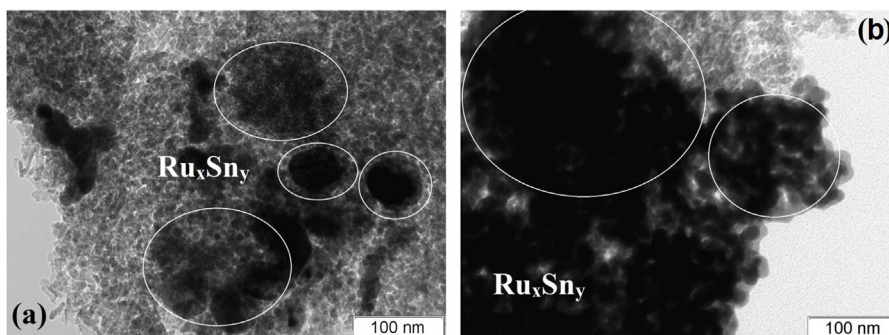

Fig. 1. TEM images of the Ru-Sn-B/Al$_2$O$_3$ samples after reaction. (A) T_{max} = 360 °C, τ = 1.67 h, P_{H_2} = 7 MPa; (B) T_{max} = 400 °C, τ = 1.67 h, P_{H_2} = 7 MPa.
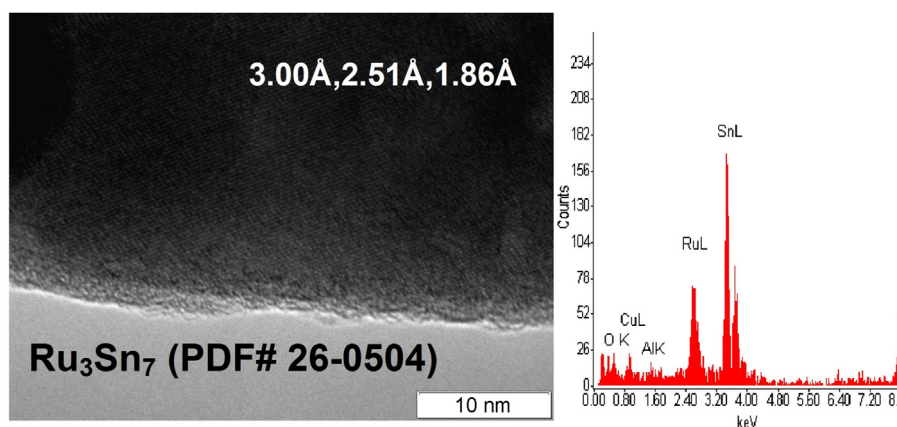
Fig. 2. High-resolution TEM image of Ru-Sn-B/Al$_2$O$_3$ sample used for the selective hydrogenation of oleic acid and the corresponding EDX data.

Table 1
Relative atomic concentrations in the subsurface layer of the Ru-Sn-B/Al$_2$O$_3$ catalysts (XPS).

Sample	$\frac{[B]}{[Al]}$	$\frac{[Ru]}{[Al]}$	$\frac{[Sn]}{[Al]}$	$\frac{[O]}{[Al]}$	$\frac{[C]}{[Al]}$	$\frac{[Na]}{[Al]}$	$\frac{[Cl]}{[Al]}$
Fresh	0.10	0.014	0.04	1.91	0.51	0.05	0.02
280 °C	0.16	0.028	0.09	1.94	0.11	0.08	0.01
310 °C	0.17	0.023	0.09	1.92	0.04	0.09	0.01
360 °C	0.18	0.018	0.08	1.85	0.02	0.09	0.01

3.1.2. X-ray photoelectron spectroscopy (XPS)

To confirm the hypothesis on the formation of crystalline aggregates when temperature increases from 280 to 320 °C, the Ru-Sn-B/Al$_2$O$_3$ catalyst samples in the oxidized state and after reduction at 280, 310 and 360 °C were analyzed by XPS. The XP-spectra of the catalyst contained peaks corresponding to Cl and Na in addition to the expected peaks of Al, B, Ru, C, Sn and O. No other impurities were observed. The presence of chlorine and sodium impurities is probably related to the use of precursors containing these elements for the catalyst synthesis [23]. Relative concentrations of the corresponding elements determined from the XPS data are reported in Table 1.

The treatment in hydrogen at 280 °C leads to an increase of the [B]/[Al], [Ru]/[Al] and [Sn]/[Al] atomic ratios, most likely, caused by the dispersion of the catalyst active component. After further treatment in hydrogen at 310 and 360 °C, the [B]/[Al] and [Sn]/[Al] atomic ratios in the catalyst do not change significantly and remain at about 0.17 and 0.09, respectively. Meanwhile, the [Ru]/[Al] ratio gradually decreases, that can indicate a growth of ruthenium-containing particles in size. This observation is in a good agreement with the results of the TEM study. The [O]/[Al] ratio does not change maintaining in a narrow range of 1.85–1.94. The value exceeds the stoichiometric ratio; this can be explained by the presence of other metal oxides and oxygenated carbon impurities. Also note that the catalyst treatment in hydrogen at high temperatures leads to gradual removal of carbon impurities from the catalyst surface ([C]/[Al] ratio, Table 1).

It shout be noted, that the method of catalysts preparation (impregnation) could probably lead to the nonuniform distribution of active component in the porous grain of the support and as a consequence the higher atomic ratios obtained by XPS. Nevertheless, the differences between absolute values of atomic ratio in the bulk and in the subsurface region does not affect the main conclusions of this work.

B1s spectra of the studied catalysts are presented in Fig. 3(a). The spectra are described sufficiently well by a single symmetrical peak with binding energy of about 192.4–192.7 eV corresponding to boron in the B^{3+} state. The B1s binding energies in the range of 192.0–193.0 eV are reported in the literature for boron in the B^{3+} state [25–28]. The catalyst reduction in hydrogen does not lead to a shift in the B1s peak position. This fact means that boron is not reduced during this treatment.

Fig. 3(b) presents the Ru3d spectra of the studied catalysts demonstrating partial overlapping of the Ru3d and C1s spectra. The 3d level in ruthenium is known to split into two sublevels Ru3d$_{5/2}$ and Ru3d$_{3/2}$ due to the spin-orbital coupling. Consequently, a Ru3d$_{5/2}$-Ru3d$_{3/2}$ doublet with a spin-orbital splitting of 4.17 eV is observed in the Ru3d spectra of the surface. The Ru3d-C1s spectrum of the fresh catalyst is described well by one Ru3d$_{5/2}$-Ru3d$_{3/2}$ doublet with the Ru3d$_{5/2}$ binding energy of 281.2 eV and three peaks related to the C1s spectrum. So high binding energy indicates that ruthenium is in the oxidized state. After the hydrogen treatment the Ru3d spectrum can be also described by a single Ru3d$_{5/2}$-Ru3d$_{3/2}$ doublet that is shifted to the region of lower energies ~278.9 eV. The shape of these peaks becomes asymmetrical. Both these facts indicate that ruthenium is reduced to the Ru^0 state. According to the literature data, ruthenium in the states Ru^0, Ru^{4+} and Ru^{6+} is characterized by Ru3d$_{5/2}$ binding energies 279.0–280.1, 280.1–281.5 and 281.8–282.8 eV, respectively. So, in the fresh catalyst ruthenium is in the Ru^{4+} state, whereas the treatment in hydrogen results in its complete reduction to the metal state.

Sn3d spectra of the studied catalysts partially overlap the NaKLL Auger peak of sodium and Ru3p$_{1/2}$ spectrum of ruthenium (Fig. 3c). A Sn3d$_{5/2}$-Sn3d$_{3/2}$ doublet with spin-orbital splitting 8.41 eV is observed in the Sn3d spectra. The Sn3d spectrum of the fresh catalyst is described well by a single Sn3d$_{5/2}$-Sn3d$_{3/2}$ doublet with the Sn3d$_{5/2}$ binding energy of 487.1 eV and three peaks attributed to sodium and ruthenium. High binding energy of this doublet suggests that tin is in the oxidized state. The hydrogen treatment results in the appearance of two additional Sn3d$_{5/2}$-Sn3d$_{3/2}$ doublets with Sn3d$_{5/2}$ binding energies about 484.1–484.2 and 485.1–485.2 eV. The doublet with the lowest energy has asymmetrical shape, which indicates that tin is reduced to the Sn^0 state. The doublet with the Sn3d$_{5/2}$ binding energy of 485.1–485.2 eV should be attributed to another oxidized state of tin. According to the literature data, tin states Sn^0, Sn^{2+} and Sn^{4+} are characterized by Sn3d$_{5/2}$ binding energies in the ranges of 484.0–485, 485–486 and 486.0–486.7 eV, correspondingly. So, the fresh catalyst contains tin in the Sn^{4+} state. The catalyst treatment in hydrogen leads to the partial tin reduction to the states Sn^{2+} and Sn^0.

The Al2p, B1s, Ru3d$_{5/2}$, Sn3d$_{5/2}$, O1s and Na1s binding energies and the fraction of reduced tin in the considered samples are reported in Table 2. The obtained results indicate that the catalyst treatment in hydrogen at 280 °C results in complete ruthenium
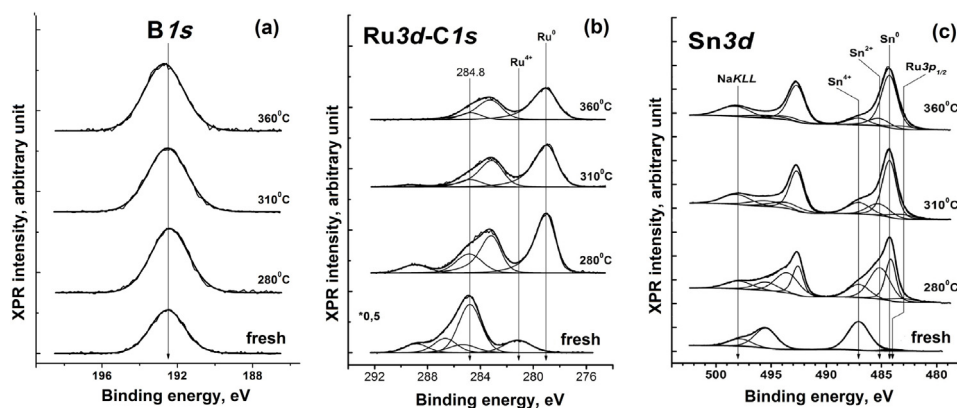
Fig. 3. B1s (a), Ru3d-C1s (b) and Sn*3d* (c) core-lever spectra of fresh and reduced Ru-Sn-B/Al$_2$O$_3$ catalysts at temperature range of 280–360 °C.

Table 2
Binding energies Al2p, B1s, Ru3d$_{5/2}$, Sn3d$_{5/2}$, O1s and Na1s, and fraction of reduced tin (in parenthesis).

Sample	Al2p	B1s	Ru3d$_{5/2}$		Sn3d$_{5/2}$			O1s	Na1s
			Ru^0	Ru^{4+}	Sn^0	Sn^{2+}	Sn^{4+}		
Fresh	74.40	192.52	–	281.18	–	–	487.07 (100)	531.49	1072.34
	75.45							532.54	
280 °C	74.40	192.41	278.92	–	484.14 (33)	485.14 (47)	487.05 (20)	531.18	1071.94
	75.30							532.08	
310 °C	74.40	192.53	278.86	–	484.25 (62)	485.26 (19)	487.05 (19)	531.21	1072.47
	75.40							532.21	
360 °C	74.40	192.71	278.94	–	484.25 (75)	485.22 (13)	487.10 (12)	531.23	1072.10
	75.27							532.10	

reduction to the metal state and partial tin reduction to states Sn^{2+} (47%) and Sn^0 (33%). Additional treatment of the catalyst in hydrogen at 310 °C leads to the two-fold increasing fraction of tin in the metal state Sn^0 (62%). Further catalyst reduction does not have a significant influence on the fraction of Sn^0 on the catalyst surface. So, the tin reduction can be assumed to have a major effect on the catalyst selectivity.

According to the TEM data, the catalyst reduction leads to the formation of a Ru$_x$Sn$_y$ solid solution of variable composition on the catalyst surface. Its concentration grows with the increase of the tin concentration in the metal state. A substantial change in the concentration of the Ru$_x$Sn$_y$ solid solution, which is the active site of the reaction, may affect the selectivity of the main reaction pathways.

3.1.3. Temperature-programmed reduction (TPR)

The TPR study was made to characterize the catalysts used for the selective hydrogenation of oleic acid to the corresponding alcohols. This method gives information on the reduction temperature of the oxidized species in the catalyst. The TPR profile of a single-metal ruthenium catalyst was found to have two characteristic reduction regions with maxima at 180 and 250 °C (Fig. 4). According to the literature data, the first region corresponds to RuCl$_2$ reduction to the metallic ruthenium [29]. The second region corresponds to the reduction of ruthenium oxychloride [30]. The TPR profile of a single-metal tin catalyst was characterized by a wide reduction range between 150 and 550 °C, which has two characteristic hydrogen-absorption regions at 150–250 °C and 350–550 °C. Such shape of the TPR profile is caused by the interaction of tin oxide with alumina. Note that Sn^{4+} species deposited on alumina were shown to be only partially reduced to Sn^{2+} due to the interaction with the support, which prevents reduction of tin ions to the metal state [31–33]. For bimetallic catalysts the region corresponding to the reduction of RuCl$_x$ forms was shifted to lower temperatures. This result can be explained by the fact that tin alters the acidity
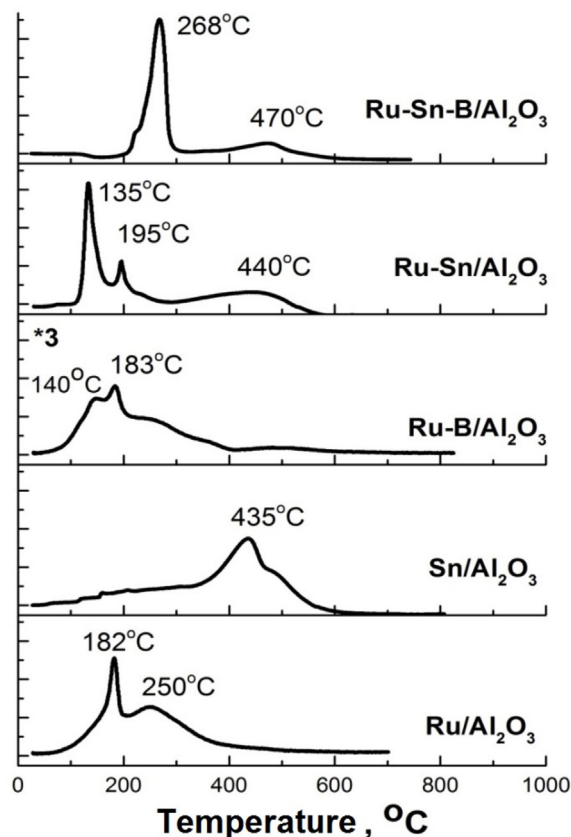

Fig. 4. TPR profiles of Ru-Sn catalysts.

of the alumina support weakening its interaction with ruthenium. The reduction region at temperatures above 400 °C can be related
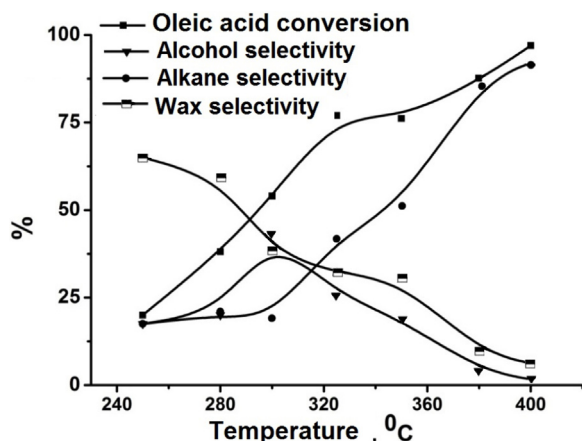
Fig. 5. Dependence of the oleic acid conversion in the presence of the Ru-Sn-B/Al_2O_3 catalyst and selectivity to the main products on temperature at $\tau = 1.67$ h, $P_{H_2} = 7$ MPa.

Fig. 6. Dependence of the oleic acid conversion in the presence of the Ru-Sn-B/Al_2O_3 catalyst and yield of the main products on hydrogen pressure at $\tau = 1.67$ h, T = 300 °C.

Fig. 7. Dependence of the selectivity to the main products on contact time at T = 300 °C, $P_{H_2} = 7$ MPa (points – experimental data, lines – simulation results using the model presented below).

to the partial tin reduction. The Ru-Sn-B/Al_2O_3 bimetallic catalyst modified by boron had an atypical peak between 250 and 280 °C with a maximum at 268 °C, which corresponds to a simultaneous reduction of ruthenium and tin oxides [14,34,35]. The elongated tail at 300–500 °C, most likely, is related to the reduction of individual tin particles [36]. Fig. 4 demonstrates that the catalyst modifying by boron facilitates reduction of the major part of tin and ruthenium oxides in the same temperature range, which is significantly lower than the reduction temperature of the single-metal tin catalyst.

According to the XPS data, Ru metal peaks and tin peaks corresponding to the forms of Sn^0 (33%), Sn^{2+} (47%), Sn^{4+} (20%) can be identified on the surface of the catalyst reduced at 280 °C (Table 2). Further rise of the catalyst reduction temperature to 310 °C substantially increases the content of tin in the metal form on the catalyst surface (up to 62%). Based on the results obtained by TPR and XPS, an optimal temperature of 300 °C was selected for preliminary reduction of the Ru-Sn-B/Al_2O_3 catalyst. At this temperature complete reduction of ruthenium oxide and substantial reduction of tin oxide to the metal states take place.

3.2. Influence of the reaction conditions on the selective hydrogenation of oleic acid on the Ru-Sn-B/Al_2O_3 catalyst

Move from static to continuous mode experiments on the selective hydrogenation of oleic acid was performed to investigate possible reaction pathways of the substrate depending on various process conditions (temperature, pressure, contact time, catalyst type, etc.). The Ru-Sn-B/Al_2O_3 catalyst that demonstrated significant activity in selective hydrogenation of fatty acid derivatives in a batch reactor [10,14,15,34–40] was used in the experiments.

The effect of the reaction temperature was studied at contact time of 1.67 h and hydrogen pressure of 7 MPa. Note that the oleic acid conversion regularly increases with temperature. Consequently, selectivity to waxes and fatty alcohols goes down (Fig. 5). Sharp decrease of the Ru-Sn-B/Al_2O_3 catalyst selectivity toward desired products may result from the agglomeration of the active component particles that was observed by the TEM study after the temperature rise from 350 to 400 °C. Taking into account all the factors, the optimal temperature range was found to be 280–330 °C.

The dependence of the oleic acid conversion and yield of the main products on the hydrogen pressure at $\tau = 1.67$ h and T = 300 °C in the presence of the Ru-Sn-B/Al_2O_3 catalyst is presented in Fig. 6. The pressure growth results in an increase of the reaction rate and, consequently, conversion. As it is shown in Fig. 6, the oleic acid conversion steadily grows with the hydrogen pressure increase. Note
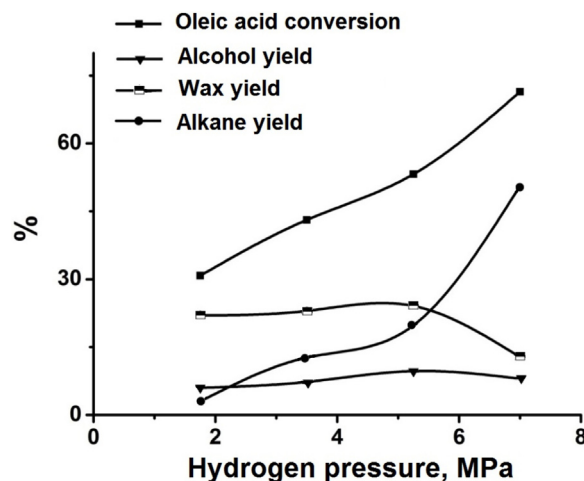
that the yield of waxes decreases when the hydrogen pressure rises, apparently, due to the growth of the contribution of its hydrocracking. In turn, this leads to higher yield of alkanes. Considering the obtained results, the optimal hydrogen pressure for selective synthesis of alcohols and waxes was concluded to be 3.5–5.3 MPa.

The effects of contact time on the oleic acid conversion and selectivity toward the main hydrogenation products at 320 °C and 7 MPa are shown in Fig. 7. Note that similar results were obtained at other reaction temperatures as well. Significant amounts of waxes (up to 60%) were formed at short contact times (<0.1 h) at 300–350 °C. They appear to be formed due to a recombination of RCOO- and R- intermediates on the catalyst surface. When the contact time was increased from 0.05 to 0.45 h, the selectivity to waxes decreased from 60 to 40%, whereas the selectivity to alkanes rose from 11 to 29%. Comparable change of selectivity can be related to the fact that alkanes are formed by the hydrocracking of waxes at these conditions. Meanwhile, the selectivity to alcohols remains constant and is about 25%. A different product distribution was observed when the reaction temperature was increased to 360 °C. In this case, the alkane selectivity rose up to 86% with the contact time growth. At high temperatures (T ≥ 350 °C) alkanes become the main reaction products (Fig. 8), which are undesirable in this study. At 360 °C the selectivity toward waxes and alcohols does not exceed 30% and tends to decrease with the contact time
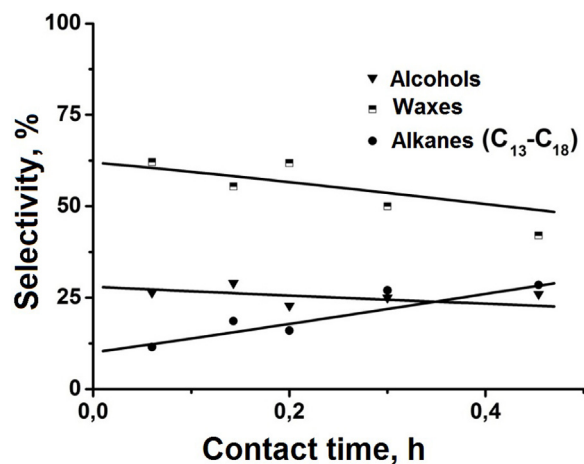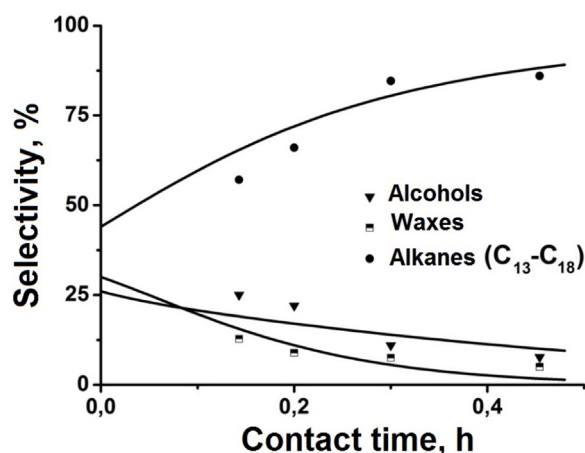
Fig. 8. Dependence of the selectivity to the main products on contact time at T = 360 °C, P_{H_2} = 7 MPa (points – experimental data, lines – simulation results using the model presented below).
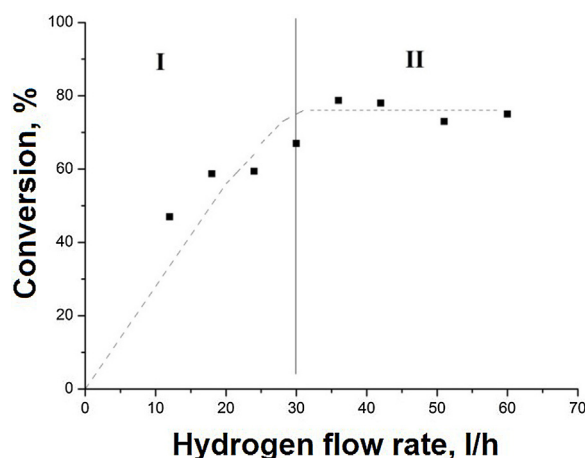

Fig. 9. Dependence of the oleic acid conversion in the presence of the Ru-Sn-B/Al$_2$O$_3$ catalyst on the gas flow rate at T = 320 °C, τ = 0.3 h, and oleic acid feed rate 20 ml/h (points – experimental data, dashed line – simulation results).

rising. Hence, an increase of temperature or contact time does not lead to the formation of desired products in selective hydrogenation of oleic acid.

3.3. Kinetic studies of the selective hydrogenation of oleic acid in the presence of Ru-Sn-B/Al$_2$O$_3$ catalyst

3.3.1. Effect of external and internal diffusion

Some preliminary experiments were carried out to estimate possible existence of external and internal diffusion limitations. Experiments on the effect of the feed gas flow rate at constant H$_2$:Ar ratio equal to 7:1 showed that volumetric ratio H$_2$/oleic acid above 1500 should be used to exclude the effect of external diffusion on selective hydrogenation of oleic acid. Therefore, the H$_2$/oleic acid ratio equal to 2100 was chosen for subsequent experiments (Fig. 9). The temperature variation within 40 °C has a minor effect on the diffusional phenomena. Thus, the obtained dependence (Fig. 9) can be expected to be valid within the whole studied temperature range.

For quantitative evaluation of the external diffusion parameters at the most critical reaction conditions (P = 8 MPa, T = 360 °C, τ = 0.3 h, oleic acid feed rate 20 ml/h, H$_2$ flow rate 43 l/h), we made an assumption that excludes the effect of the substrate. With this

assumption, the observed reaction rate under isothermal conditions does not deviate by more than 5% if inequality (1) is met.

$$\frac{k_{\text{исх}}c_o r_p}{c_0 k_c} < \frac{0,15}{n} \tag{1}$$

Here r_p is the catalyst grain size (3×10^{-4} m), c_p is the reagent concentration (molar fraction) at the reactor inlet, k_c is the coefficient of mass transfer between the gas flow and the grain, which is a function of the Schmidt and Reynolds numbers, n is the reaction order (n = 1), k_{in} is the reaction rate constant at T = 360 °C.

At 360 °C as well as at all other studied temperatures and linear hydrogen flow rate 8 cm/s, the left part of inequality (1) is equal to 0.0074, which is significantly lower than 0.15. This result indicates that the effect of external diffusion at the used reaction conditions is minimal.

The effect of internal diffusion on the reaction rate is characterized by the efficiency factor η determined as the ratio of the observed reaction rate to the rate that would be observed in the absence of diffusion phenomena in the catalyst pores. The efficiency factor is a function of the Thiele modulus. Internal diffusive effect can be assessed using the Thiele modulus criterion. The effect of diffusion in pores is considered to be insignificant if the Thiele modulus φ is smaller than 1 (2).

$$\varphi = r_p \sqrt{\frac{k_{\text{исх}}}{D_{\text{эф}}}} \tag{2}$$

Here φ is the Thiele modulus, k_{in} is the reaction rate at T = 360 °C, D_{ef} is the effective hydrogen diffusion coefficient, r_p is the catalyst grain size (3×10^{-4} m).

At the chosen process conditions, the Thiele modulus is equal to 0.02. As this value is substantially smaller than 1, we can assume that at these conditions the reaction rates are controlled by kinetics.

3.3.2. Determination of kinetic parameters for the selective hydrogenation of oleic acid

Six sets of experiments with different quantities of the catalyst and temperature variation during the reaction were carried out. To avoid changes of the reagent distribution in the catalyst bed and its hydrodynamics, a fresh catalyst sample of the same volume was used in each experiment, the substrate feed rate (20 ml/h) and gas flow rates (H$_2$–43 l/h, Ar – 6 l/h) were kept constant. The substrate feed rate and the gas flow rates were selected to observe formal excess of hydrogen (ν (H$_2$)/ν (oleic acid) = 30 mol/mol). During formal kinetic evaluations, the oleic acid hydrogenation reaction was assumed to be of pseudo-first substrate reaction order.

The dependence of the oleic acid conversion on contact time at different temperatures presented in Fig. 10 shows that the temperature increase from 250 to 360 °C leads to the substrate conversion rise at each contact time. The maximum conversion (99%) was observed at the temperature of 360 °C and contact time of 0.454 h.

Kinetic parameters were estimated using mathematical methods. Reaction rate constants of oleic acid deoxygenation at different temperatures and contact times were determined by analytical solution of the equation of the substrate consumption:
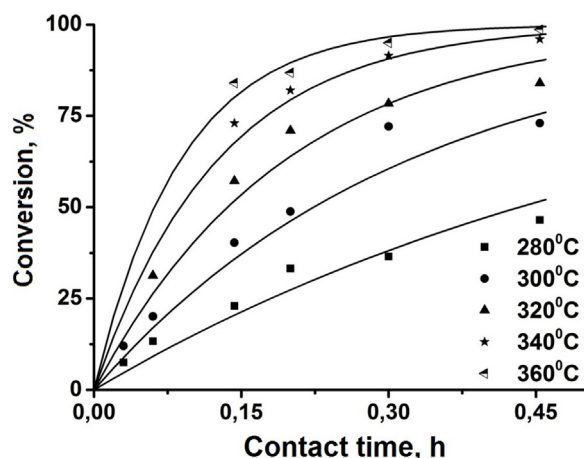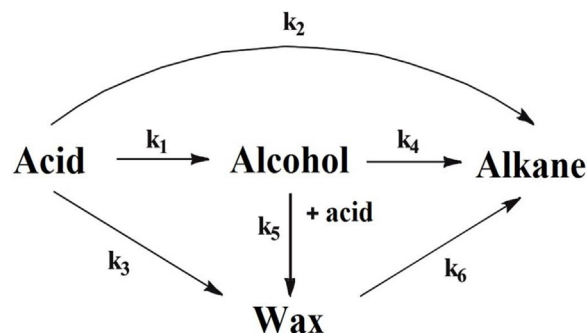
$$C_A = C_0 e^{-K\tau} \tag{3}$$

where the boundary conditions: τ = 0, C_0 = 1, the C_A = 0, where τ – contact time, h; K – rate constant consumption of oleic acid in total of all routes transformation, h^{-1}; C_A – concentration (molar fraction) of oleic acid; C_0 – initial concentration (molar fraction) of oleic acid.

Obtained data allowed us to estimate the activation energy of this stage as 69 ± 4 KJ/mol. These results are in a good agreement with the data of M. Sánchez et al. [41].

Table 4
Kinetic parameters of oleic acid selective hydrogenation in the presence of the Ru-Sn-B/Al$_2$O$_3$ catalyst at P$_{H_2}$ = 7 MPa.

	k_1	k_2	k_3	k_4	k_5	k_6
k_{oi}	4.4*10^5 (h^{-1})	4.4*10^{11} (h^{-1})	365 (l/h mol^{-1})	4.4*10^5 (h^{-1})	2.2*10^4 (l/h mol^{-1})	9.7*10^9 (h^{-1})
E_a (kJ/mol)	62 ± 9	133 ± 5	24 ± 7	64 ± 1	54 ± 2	110 ± 8

Fig. 10. Dependence of the oleic acid conversion in the presence of the of Ru-Sn-B/Al$_2$O$_3$ catalyst on contact time at T = 280–360 °C, P$_{H_2}$ = 7 MPa (points – experimental data, lines – simulation results using the model presented below).

Fig. 11. Kinetic scheme of the oleic acid hydrodeoxygenation in the presence of the Ru-Sn-B/Al$_2$O$_3$ catalyst at P$_{H_2}$ = 7 MPa.
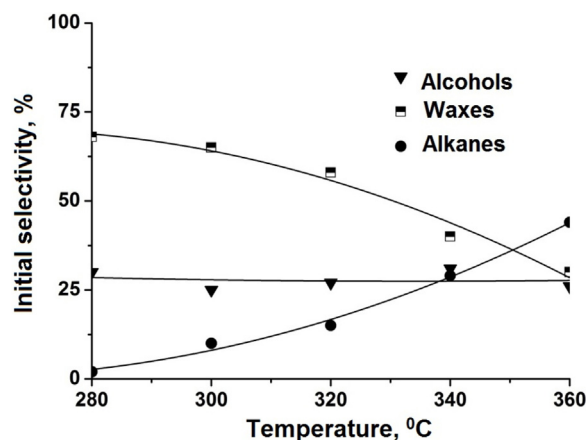
A kinetic scheme for the selective hydrogenation of oleic acid based on the regularities described above was suggested. It includes the stages of direct acid hydrodeoxygenation to alkanes, hydrocracking of waxes to alkanes and formation of waxes (Fig. 11).

The suggested kinetic scheme presumes parallel oleic acid conversion to fatty alcohols (k$_1$), n-alkanes (k$_2$) and waxes (k$_3$). Total rates of the reagent consumption by all these pathways are reported in Table 4. Direct formation of alkanes from carboxylic acids involves decarboxylation reaction with the decrease of the chain length of the formed alkane by one carbon atom. So, heptadecane C$_{17}$H$_{36}$ is the main product. Then, alcohols are transformed either to waxes by the esterification with the initial acid (k$_5$) or to alkanes by deoxygenation (k$_4$). Moreover, in this scheme hydrocracking of waxes to form alkanes (k$_6$) have to be taken into account. Special attention should be paid to the formation of alkanes and waxes from acids and to hydrocracking of waxes as these stages obtained on the basis of our experimental data have not been widely discussed in the literature before.

As the reaction may involve high substrate conversions, a model of plug-flow reactor taking into account variation of the reaction mixture composition was used for evaluation of the kinetic constants. The constants at different temperatures and contact times

Table 3
Reaction rate constants of different stages of oleic acid selective hydrogenation in the presence of the Ru-Sn-B/Al$_2$O$_3$ catalyst at P$_{H_2}$ = 7 MPa.

Temperature, °C	k_1, h^{-1}	k_2, h^{-1}	k_3, l/h mol^{-1}	k_4, h^{-1}	k_5, l/h mol^{-1}	k_6, h^{-1}
280	0.48	0.03	1.1	0.1	0.08	1.4
300	0.9	0.3	2	0.6	0.3	0.9
320	1.4	0.8	3	1	0.45	2.6
340	2.8	2	3.2	1.6	0.7	5.5
360	3	5	3.4	2.3	0.92	9

Fig. 12. Dependence of the initial selectivity to the main products in the presence of the Ru-Sn-B/Al$_2$O$_3$ catalyst on temperature at P$_{H_2}$ = 7 MPa.

were obtained by the Kutta-Merson method (4) with boundary conditions $l = 0$: $C_i = C_i^0$, U = 1.

$$\frac{dC_i}{d\tau} = \frac{F_i - C_i \cdot \sum F_i}{U}$$
$$\{ \frac{dU}{d\tau} = \sum F_i$$
$$F_i = \sum_k^{N_r} \nu_{ki} \cdot r_k$$
(4)

Here r_k is the rate of the k-th reaction written in accordance with the law of mass action, 1/s; F_i is the consumption rate of the i-th component, 1/s; C_i is the molar fraction of the i-th component; τ is contact time, s; ν_{ki} is the stoichiometric coefficient of the i-th component in k-th reaction; and U is the ratio of the current molar flow rate to the input one.

The obtained simulation results adequately describe the experimental data (Figs. 7 and 8). Based on the reported above model of the reagent concentration dependence on the contact time the reaction rate constants of the stages in the scheme assumed for the selective hydrogenation of oleic acid (Fig. 11) were calculated (Table 3).

Using the mathematical model and the obtained rate constants (Table 3), the experimental data were extrapolated to zero contact time (Fig. 12). This extrapolation allowed us to obtain the dependence of the initial selectivity toward all products (alcohols, waxes, acids) on temperature.
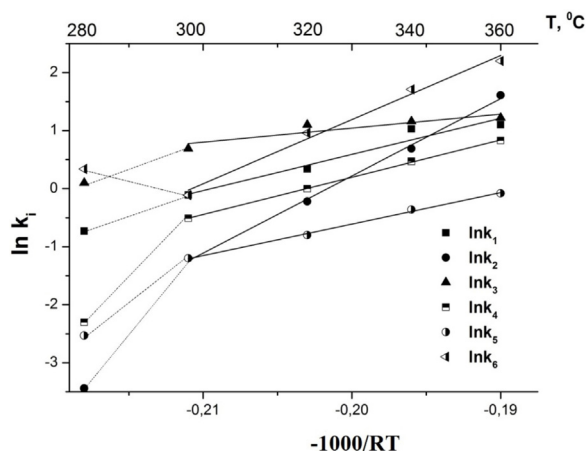
Fig. 13. Dependence of the reaction rate constants of different stages during selective hydrogenation of oleic acid on reverse temperature (points – calculated data, lines – approximation results, dashed lines – region not taken into account during the calculations).

Fig. 12 demonstrates that the wax formation reaction has the main contribution to conversion of the acid substrate in the temperature range of 280–340 °C. At higher temperatures the process shifts to the formation of alkanes. Also note that the initial selectivity to alcohols practically does not depend on temperature. This result may be related to proportional change of components content in the liquid sample.

Based on the obtained rate constants (Table 3), the dependences of the reaction rate constants for each stage of the selective oleic acid hydrogenation on reverse temperature in Arrhenius coordinates were plotted (Fig. 13).

The obtained data were used to estimate the main kinetic parameters (k_0, E_a) for each stage of selective hydrogenation at $P_{H2} = 7$ MPa in the presence of the Ru-Sn-B/Al$_2$O$_3$ catalyst. The obtained results are reported in Table 4.

The highest activation energy was found for the formation of alkanes from the acid (k_2). This result suggests that this reaction stage most significantly depends on temperature. The reaction rate constant for the formation of alcohols (k_1) rises threefold (from 0.9 to 3.0 h^{-1}) when the temperature increases from 300 to 360 °C. Meanwhile, the wax formation rate ($k_3 + k_5$) is the least dependent on temperature growing and changes from 2.3 to 4.32 h^{-1} only, which is confirmed by the low activation energy values.

The kink in the rate constant dependences observed between 280 and 300 °C (Fig. 13) can be explained by a reaction mechanism change. The XPS study of the catalyst reported above showed that the reduction of the Ru-Sn-B/Al$_2$O$_3$ catalyst in hydrogen at 280 °C results in complete ruthenium reduction to the metal state and only partial tin reduction to Sn^{2+} (47%) and Sn^0 (33%). Further catalyst treatment at 310 °C leads to a significant increase in the concentration of reduced tin Sn^0 (62%). As a consequence, the reaction mechanism can change causing the kink observed in Fig. 13. Furthermore, it was shown by TEM that crystalline Ru$_x$Sn$_y$ aggregates are not formed at the catalyst reduction stage. However, such aggregates were observed in the samples of the catalyst after reaction at high temperatures (340–360 °C). This result indicates that both the oxidation state and the phase composition of the catalyst changes at high temperatures leading to changes in its activity and selectivity.

In general, the obtained experimental data are correctly described by the suggested kinetic model (Figs. 10, 12 and 13). So, the investigation of the Ru-Sn-B/Al$_2$O$_3$ catalyst by physicochemical methods and quantitative evaluation of the suggested reaction pathways for oleic acid conversion to alcohols, waxes and alkanes allowed us to determine the relationship between the nature of the catalyst active component and its activity and selectivity at different reaction conditions.

5. Conclusions

Several physicochemical methods including *in situ* regimes were used to study samples before and after reaction in order to determine the composition of the catalyst active component and its effect on the activity and selectivity of the catalytic system in general. It was shown by TPR that modifying the Ru-Sn-B/Al$_2$O$_3$ catalyst with boron promotes additional simultaneous reduction of the major part of tin and ruthenium oxides, most of which are reduced below 300 °C. According to the XPS data, small ruthenium metal particles and tin in the states Sn^0 (33%), Sn^{2+}(47%), and Sn^{4+}(20%) are identified on the surface of the Ru-Sn-B/Al$_2$O$_3$ catalyst at 280 °C. The catalyst reduction at 310 °C enhances the fraction of metal tin on the surface up to 62%. An optimal temperature equal to 310 °C was selected for preliminary reduction of the Ru-Sn-B/Al$_2$O$_3$ catalyst based on the TPR and XPS data. At this temperature all ruthenium and most of tin are reduced to the metal states. It was shown by TEM that after the catalyst reduction the Ru$_x$Sn$_y$ phase was in a truly amorphous state before reaction. Crystalline Ru$_x$Sn$_y$ structures with variable composition, which seem to be the active component of the selective hydrogenation catalyst, were observed to be formed after reaction at higher temperatures. The active component particles were noted to agglomerate with the reaction temperature increase. Therefore, the selective hydrogenation of fatty acids in the presence of the Ru-Sn-B/Al$_2$O$_3$ catalyst should be performed at the temperatures equal or lower 350 °C.

Investigation of the parameters used for the selective hydrogenation of oleic acid in the continuous flow mode in the presence of the Ru-Sn-B/Al$_2$O$_3$ catalyst showed that the process should be performed at the temperature range of 280–330 °C, hydrogen pressure of 3.5–5.3 MPa and contact time less than 0.2 h in order to obtain the highest possible yield of desired products (fatty alcohols and waxes). It was shown that change of the active component oxidation state on the catalyst surface depending on the reaction temperature can directly affect the catalyst activity and selectivity.

A scheme of oleic acid transformations was suggested on the basis of the obtained product distribution. It includes additional hydroconversion stages that were not considered for this process in the literature before, namely, formation of waxes by recombination of carboxyl and alkanes intermediates, acid decarboxylation and hydrocracking of waxes to alkanes. Mathematic simulation methods were used to develop a kinetic model, estimate rate constants of the process stages and main kinetic parameters (E_a, k_0). The suggested model gives quite a good description of the experimental data and can be used for further development of the process and its scaling up.

References

[1] Eurasian chemical market 51 (2009) 50–60.
[2] K. Noweck, W. Grafahrend, Ullmann's Encyclopedia of Industrial Chemistry, Wiley-VCH Verlag GmbH & Co KGaA, Weinheim, 2000.
[3] U. Kreutzer, J. Am. Oil Chem. Soc. 61 (1984) 343–348.
[4] T. Voeste, H. Buchold, J. Am. Oil Chem. Soc. 61 (1984) 350–352.
[5] H.C. Eckstrom, J. Chem. Educ. 40 (1963) A146.
[6] V. Satagopan, S.B. Chandalia, J. Chem. Technol. Biotechnol. 59 (1994) 257–263.
[7] V. Satagopan, S.B. Chandalia, J. Chem. Technol. Biotechnol. 60 (1994) 17–21.

[8] J. Kašpar, M. Graziani, G.P. Escobar, A. Trovarelli, J. Mol. Catal. 72 (1992) 243–251.
[9] J. Ross, J. Appl. Catal. 22 (1986) 398.
[10] V.M. Deshpande, K. Ramnarayan, C.S. Narasimhan, J. Catal. 121 (1990) 174–182.
[11] F. Mizukami, S. Niwa, M. Toba, T. Tsuchiya, K. Shimizu, S. Imai, J. Imamura, Stud. Surf. Sci. Catal. 31 (1987) 45–54.
[12] K.Y. Cheah, T.S. Tang, F. Mizukami, S.I. Niwa, M. Toba, Y.M. Choo, J. Am. Oil Chem. Soc. 69 (1992) 410–416.
[13] C.S. Narasimhan, V.M. Deshpande, K. Ramnarayan, J. Appl. Catal. 48 (1989) L1–L6.
[14] Y. Pouilloux, F. Autin, C. Guimon, J. Barrault, J. Catal. 176 (1998) 215–224.
[15] Y. Pouilloux, A. Piccirilli, J. Barrault, J. Mol. Catal. A.: Chem. 18 (1996) 161–166.
[16] Y. Pouilloux, F. Autin, A. Piccirilli, C. Guimon, J. Barrault, Appl. Catal. A.: Gen. 169 (1998) 65–75.
[17] Y. Pouilloux, F. Autin, J. Barrault, Catal. Today 63 (2000) 87–100.
[18] M.A. Sánchez, V.A. Mazzieri, M.R. Sad, R. Grau, C.L. Pieck, J. Chem. Technol. Biotechnol. 86 (2011) 447–453.
[19] K. De Oliveira, Y. Pouilloux, J. Barrault, J. Catal. 204 (2001) 230–237.
[20] J.H. Scofield, J. Electron Spectrosc. 8 (1976) 129–137.
[21] Ch. Setterfield, Practical course of heterogeneous catalysis, Mir, Moscow, 1984.
[22] T. Miyake, T. Makino, H. Watanuki, T. Niki, S. Shimizu, Y. Kojima, M. Sano, Appl. Catal. A.: Gen. 364 (2009) 108–112.
[23] D.A. Echeverri, J.M. Marín, G.M. Restrepo, L.A. Rios, Appl. Catal. A.: Gen. 366 (2009) 342–347.
[24] V.M. Deshpande, W.R. Patterson, C.S. Narasimhan, J. Catal. 121 (1990) 165–173.
[25] W.-L. Dai, M.-H. Qiao, J.-F. Deng, J. Appl. Surf. Sci. 120 (1997) 119–124.
[26] J.C. Read, P.G. Mather, R.A. Buhrman, J. Appl. Phys. Lett. 90 (2007) 132.
[27] D.V. Savchenko, A.A. Serdan, V.A. Morozov, G. Van Tendeloo, S.G. Ionov, J. New Carbon Mater. 27 (2012) 12–18.
[28] D.J. Joyner, D.M. Hercules, J. Chem. Phys. 72 (1980) 1095–1108.
[29] V. Mazzieri, F. Coloma-Pascual, A. Arcoya, P.C. L'Argentière, J. Appl. Surf. Sci. 210 (2003) 222–230.
[30] A. Bossi, F. Garbassi, A. Orlandi, G. Petrini, L. Zanderighi, Stud. Surf. Sci. Catal. 3 (1979) 405–416.
[31] V.A. Mazzieri, J.M. Grau, J.C. Yori, C.R. Vera, C.L. Pieck, Appl. Catal. A.: Gen. 354 (2009) 161–168.
[32] R. Burch, J. Catal. 71 (1981) 348–359.
[33] B.A. Sexton, A.E. Hughes, K. Foger, J. Catal. 88 (1984) 466–477.
[34] M.A. Sánchez, Y. Pouilloux, V.A. Mazzieri, C.L. Pieck, Appl. Catal. A.: Gen. 467 (2013) 552–558.
[35] M.A. Sánchez, V.A. Mazzieri, M.R. Sad, R. Grau, C.L. Pieck, J. Chem. Technol. Biotechnol. 86 (2011) 447–453.
[36] M. Sánchez, V. Mazzieri, M. Sad, C. Pieck, React. Kinet. Mech. Catal. 107 (2012) 127–139.
[37] K. Tahara, E. Nagahara, Y. Itoi, S. Nishiyama, S. Tsuruya, M. Masai, Appl. Catal. A.: Gen. 154 (1997) 75–86.
[38] M.J. Mendes, O.A. Santos, E. Jordão, A.M. Silva, Appl. Catal. A.: Gen. 217 (2001) 253–262.
[39] P. Kluson, L. Cerveny, Appl. Catal. A.: Gen. 128 (1995) 13–31.
[40] M.A. Sánchez, V.A. Mazzieri, M.A. Vicerich, C.L. Pieck, J. Chem. (2015) 1–7.
[41] M. Sánchez, V. Mazzieri, M. Sad, C. Pieck, React. Kinet. Mech. Catal. 107 (2012) 127–139.